IMAV2016-19
http://www.imavs.org/pdf/imav.2016.19

Electric Propulsion System Characterization through Experiments

Gautier Hattenberger*, Antoine Drouin* and Murat Bronz*
University of Toulouse ; ENAC; F-31077 Toulouse, France

ABSTRACT

Electrical propulsion system characteristics are very important in UAV design, operation and control. This article presents the characterization of electric propulsion sets through experiments. A motor test bench have been build based on previous experience in order to improve the quality of the measurements. Moreover, the bench fits in a wind tunnel, allowing to perform a complete characterization over the full airspeed range of the considered mini and micro-UAVs. After recalling the general theoretical model of an electric motor, results from various combinations are presented.

1 INTRODUCTION AND MOTIVATIONS

Electrical propulsion system characteristics are very important in Unmanned Air Vehicle (UAV) design, operation and control. They have a strong impact on the consumption and therefore on the overall performances of the system in terms of range and endurance. Several models can be found in the literature [1] for continuous current motors or brushless motors. The second type is the most commonly used on mini and micro UAVs for their superior efficiency. Manufacturers are usually providing sufficient information to estimate the main characteristics of their products, however these data are sometimes optimistic regarding the real performances of the motors. Likewise, basic information provided for propellers are only the diameter and pitch values which are not sufficient for estimating the real performance values. Some other elements can effect the overall propulsive and electrical efficiency like the choice of propeller's material and electronic speed controllers (ESC).

For the *SkyScanner* project[1] [2], which deploys a fleet of mini-UAVs in order to study the evolution of clouds, several tasks require a good knowledge of the aircraft performances. It is especially the case of the trajectory planning algorithms and the wind estimation algorithms. This paper presents the experimental setup and results of a propulsion test bench which has been developed in order to build an accurate database for several motors and propellers. These information can be used for the design process [3, 4], for model-based control methods or for improving the estimation of other parameters like the wind or the aircraft performances [5]. The measurements of the propulsion system parameters need to be done at both zero speed for the static characteristics, and also over the complete airspeed range. Then, the propulsion test bench have been designed to be used inside a wind tunnel. Due to the available wind tunnel test section size, propellers only smaller than 12 inches can be tested, hence the force sensors that are used for thrust and torque measurements are selected accordingly.

The first sections will present the propulsion model and the experimental setup designed in-house. Finally, the experimental results are presented and discussed.

2 PROPULSION MODEL

2.1 Electric Motor

Basically, electric motors are electromechanical machines that converts electrical input power into mechanical output power. The general power supply used in the UAVs is DC (Direct Current) so DC motors will be investigated in this paper. Most common types are brushed and brushless motors. Brushed motors use mechanical and brushless motors use electronic commutation in order to change the direction of electric current and generate a pulling magnetic force between the stator and the magnets. Brushless motors have numerous advantages such as having a higher efficiency than brushed motors, longer lifetime, generating less noise, having higher power to weight ratio. Therefore they are more reliable for the UAV applications.

The important task is to choose the suitable motor for the specified mission requirements. In order to be able to select the correct motor, the characterization is a must to have.

Therefore, a first order simplified model using three motor constants, and experimentally obtained characteristics of DC motors will be explained in this section. Figure 2 shows an equivalent circuit model of an electric motor.

As described in [1], the resistance R of the motor is assumed to be constant and the motor shaft torque Q_m is proportional to the current i according to motor torque constant K_Q. The friction based losses can be represented by the no load current i_0 as a subtraction.

$$Q_m(i) = (i - i_0)/K_Q \tag{1}$$

Internal voltage v_m is assumed to be proportional to the rotation rate Ω according to the speed constant K_v of the mo-

*firstname.lastname@enac.fr
[1] https://www.laas.fr/projects/skyscanner/

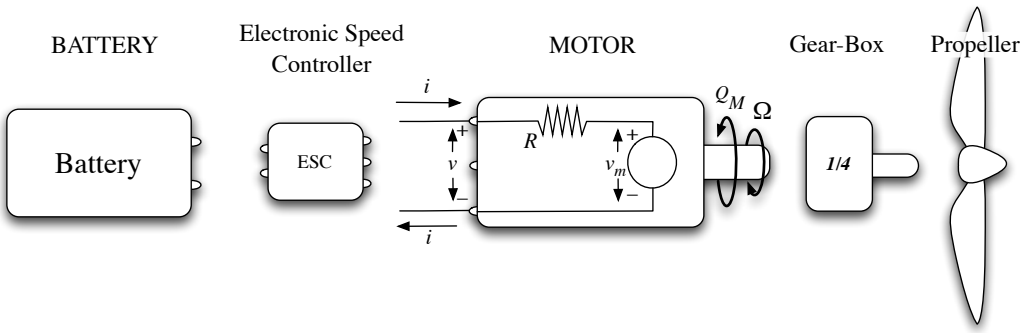

Fig. 1: Elements of a generic electric propulsion system.

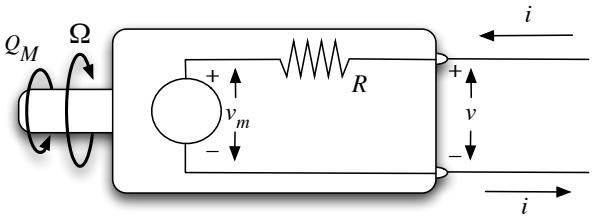

Fig. 2: Equivalent circuit for a DC electric motor[1].

tor.

$$v_m(\Omega) = \Omega / K_v \tag{2}$$

Then the motor terminal voltage can be obtained by adding the internal voltage and the resistive voltage drop.

$$v(i,\Omega) = v_m(\Omega) + iR = \Omega / K_v + iR \tag{3}$$

The above model equations can be rewritten in order to give power, torque, current and efficiency as a function of terminal voltage and rotation rate of the motor. Firstly, the current function is obtained from equation 3.

$$i(\Omega, v) = \left(v - \frac{\Omega}{K_v}\right)\frac{1}{R} \tag{4}$$

Then the others follow ;

$$Q_m(\Omega, v) = \left[i(\Omega, v) - i_0\right]\frac{1}{K_Q} = \left[\left(v - \frac{\Omega}{K_v}\right)\frac{1}{R} - i_0\right]\frac{1}{K_Q} \tag{5}$$

$$P_{shaft}(\Omega, v) = Q_m \Omega \tag{6}$$

$$\eta_m(\Omega, v) = \frac{P_{shaft}}{iv} = \left(1 - \frac{i_0}{i}\right)\frac{K_v}{K_Q}\frac{1}{1 + iRK_v/\Omega} \tag{7}$$

where P_{shaft} is the mechanical power on the shaft, K_v is usually given in RPM/Volt in motor specifications, however here it is taken as rad/s/Volt and K_Q is taken in Amp/Nm. It should be also noted that $K_Q \approx K_v$.

By knowing the first order motor constants (K_v, K_Q, i_0, R) of any off the shelf motor, the theoretical characteristic plots can be obtained by using above equations.

2.2 Propeller

The propeller is a rotating wing which utilizes the mechanical power input in order to accelerate the air particles to generate thrust. The basics of characterization of the propeller is included here, however a deeper explanation can be found in [6] and [7]. The thrust, power and torque coefficients are used to characterize a propeller, which depend on the advance ratio J (which can be found noted λ, eventually with a factor π compared to J), the average blade Reynolds number Re, and the geometry of the propeller. They are respectively defined as:

$$C_T = C_T(J, Re, geometry) \tag{8}$$

$$C_P = C_P(J, Re, geometry) \tag{9}$$

$$C_Q = C_Q(J, Re, geometry) \tag{10}$$

Reynolds number (R_e) of the propeller is defined as:

$$R_e = \frac{\rho\, \Omega R_b\, c_{ave}}{\mu} \tag{11}$$

where c_{ave} is the average chord length, ρ is the fluid density, μ is the dynamic viscosity, and R_b is the propeller blade radius. With all this parameters being constant, R_e becomes a function of the rotation speed Ω.

Advance ratio depends on the flight velocity V, and the propeller rotation speed

$$J(\Omega, V) = \frac{V}{nD} = \frac{V\pi}{\Omega R_b} \tag{12}$$

where $n = 2\pi\ \Omega$ is the number of revolutions per second and D is the propeller diameter.

Once the thrust C_T, power C_P and torque C_Q coefficients of the propeller are specified, the thrust and torque of the propeller can be calculated for any rotation rate and velocity as in [7],

$$T(J, \Omega) = T(\Omega, V) = \rho n^2 D^4 C_T(J, R_e) \tag{13}$$

$$P(J, \Omega) = P(\Omega, V) = \rho n^3 D^5 C_P(J, R_e) \tag{14}$$

$$Q(J,\Omega) = Q(\Omega,V) = \rho n^2 D^5 C_Q(J,R_e) \quad (15)$$

Finally, the efficiency of the propeller at any condition can be found as,

$$\eta_{propeller}(\Omega,V) = \frac{T\,V}{P} = \frac{T\,V}{Q\,\Omega} = \frac{J\,C_T}{2\pi\,C_P} \quad (16)$$

3 Experimental setup

3.1 Previous design

In order to study the propulsion system performances, a preliminary test bench has been designed [5], resulting in promising results, but also with several flaws. This bench, shown in figure 3, was constructed with pre-formed aluminum bars and assembled 3D printed plastic (ABS) pieces. Two force sensors were used in order to measure the propulsion force and torque. A custom electronic board was measuring the electrical current and voltage, and the motor RPM as well. In addition, a Pitot tube placed in front was giving the wind tunnel speed. The complete testing procedure was controlled by a *MyRIO* data acquisition board from *National Instruments* and a *LabView* graphical interface.

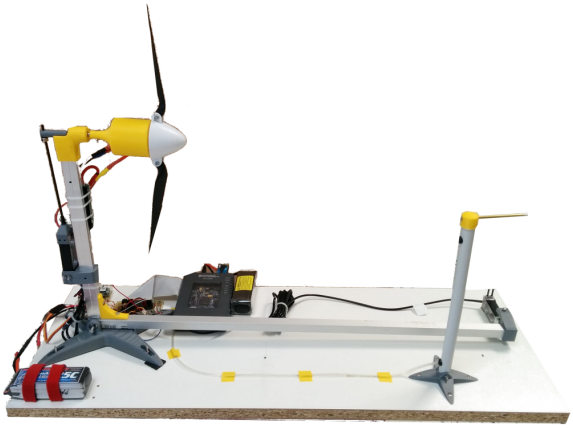

Fig. 3: First test bench version.

This first design gave promising results as shown on figure 4, where the thrust is displayed as a function of the motor RPM for different airspeed. These tests have nevertheless showed some limitations. In particular, some combinations of motors and propellers were producing strong vibrations leading to false measurements.

The main reason was the rather fragile mechanical mounting of the bench. An other source of error was the position of the sensors. Their sensitivity and size were imposing to have them far from the tested motor, at the tip of the bottom aluminum bar for the thrust and using a 10 cm carbon rod at the back of bench for the torque. With longer connection, the vibrations were greatly increased at some airspeed and RPM combinations. The electric sensors (voltage, current, RPM) were integrated on custom electronic boards using rather long cables, which adds some measurement noise.

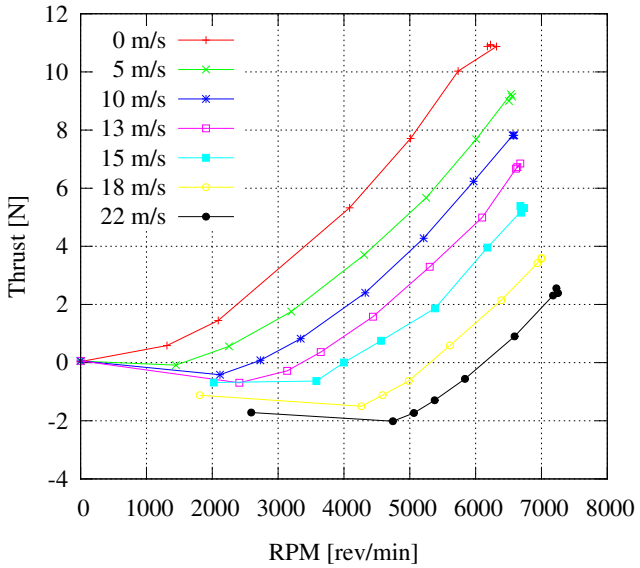

Fig. 4: Thrust versus RPM at different airspeed from wind tunnel experiment.

3.2 Current Propulsion Test Bench

Keeping in mind the previous design flaws, the new test bench has been designed accordingly while giving more attention to the below mentioned items:

- the structure should be stiffer
- the force and torque sensors should be placed closer to the motor and propeller
- the electric sensors should have a better integration
- optionally, the amount of sensors used has to be reduced.

Figure 5 shows the new version of the propulsion test bench inside the wind tunnel of ENAC (French Civil Aviation University) that is build based on these considerations. The wind tunnel has a 0.5m by 0.5m open test section with 1 meter long. It is mainly used for instructional purpose for the aviation students, however it is still suitable to be used for research purposes. Figure 6 shows the detailed CAD drawing where the sensors are placed directly to the main shaft holding the motor and propeller couple to reduce the additional structural vibrations. The two force sensors that are used for thrust and torque measurements are respectively SMD2207-050 and SMD2207-020 from *strain measurement devices*.[2] The main shaft is free to move forward and backward and also rotates freely in order to transfer force and moments directly to the sensors. The linear and rotational motion is obtained by using thin wall bearings FMT-012 from *PCB*.[3] The main

[2] www.smdsensors.com
[3] www.pcblinear.com

shaft is free to rotate and translate, however it is held by the sensors measuring the thrust and torque. Hence the moment of inertia of the main shaft has no impact on the measurements. The clean integration of the sensors and the power cables to the main test bench mast minimize their additional effects on the measurements.

The speed controller used for the new test bench is ESC32v3[4]. The main reason is that it can directly give the motor voltage, the current draw, and the RPM via a serial link, so that reducing the number of required sensors on the system.

Finally the bench is fixed on a wooden plate placed in the wind tunnel test section, where the length can vary in order to fit into bigger wind tunnel test sections.

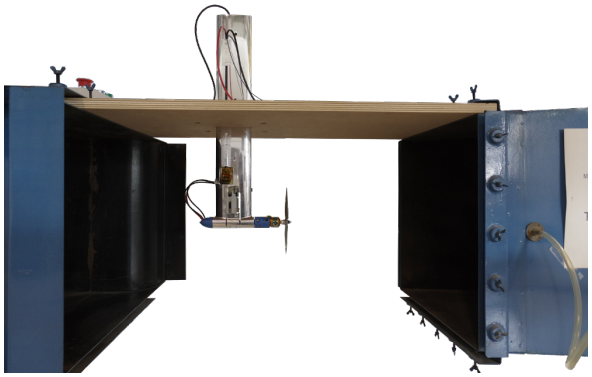

Fig. 5: Improved new test bench version inside the wind tunnel.

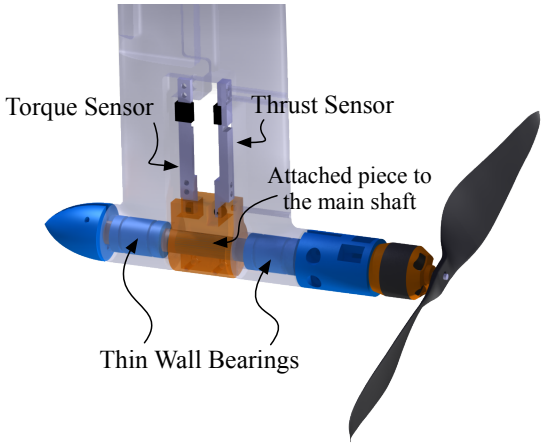

Fig. 6: The detailed CAD view of the sensor integration used in the new version of propulsion test bench.

3.3 Calibration Process

Calibration of the sensors is one of the most important issues for the correct measurements. Usually this process is difficult to make and done only once in a while. However, it has been observed that after the replacement of propeller or motor, the torque sensor is getting effected and changing its calibration values. In order to overcome this problem, and make sure that the test bench is well calibrated at each experiment, easy to attach and remove clip-on calibration parts have been designed. The attached pieces are shown in Figure 7.

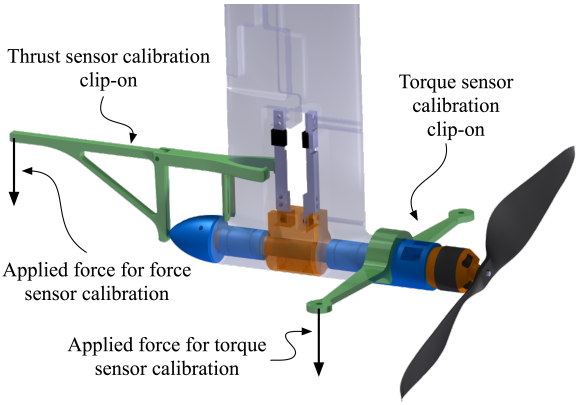

Fig. 7: Clip-on calibration parts.

The objective while designing the clip-on parts was to make the calibration process as easy and fast as possible. On the graphical user interface, the calibration window consists of several predefined loading values. After placing the clip-on to its designated location, the user starts applying the predefined load from the locations that are shown in Figure 7. A dynamic point, moving in real-time on the graph, shows the location of the load value versus raw values. The user can go over all the predefined loads and recalibrate the sensor, or just use the graph in order to check the fit of calibration curves for any given loading.

One of the calibration steps consists of subtracting the motor and shaft drag, when there is no propeller, from the measurements. Thanks to the design of the test bench this correction remains very low.

A particular problem that has been encountered was the static friction of the thin wall bearings. During the calibration, the small loadings would not overcome the static friction of the system and became *invisible* to the sensors. This has been solved by adding a small vibration to the system. The motor is rotated really slowly, so slowly that it does almost not generate any thrust, however the phase changes of the magnets on the motor vibrates the shaft. This effect naturally exists during all the real tests and was sufficient to overcome the static friction so that even the smallest loads such as 0.05 N can be used during the calibration process.

[4] www.autoquad.org/esc32/

4 RESULTS

4.1 *Thrust, Power and Torque Coefficients*

The C_T, C_P and C_Q coefficients can be generated from the measurements using equations 13, 14 and 15. In addition, we assume that in the useful range of flight speed (around 10 to 20 m/s), these coefficients can be linearized as follow:

$$C_T(J,\Omega) = \frac{T}{\rho n^2 D^4} = C_{T_0} + C_{T_J} J + C_{T_{RPM}} RPM \qquad (17)$$

$$C_P(J,\Omega) = \frac{P}{\rho n^3 D^3} = C_{P_0} + C_{P_J} J + C_{P_{RPM}} RPM \qquad (18)$$

$$C_Q(J,\Omega) = \frac{Q}{\rho n^2 D^5} = C_{Q_0} + C_{Q_J} J + C_{Q_{RPM}} RPM \qquad (19)$$

where $C_{\{T,P,Q\}_{\{0,J,RPM\}}}$ are constant coefficients. This assumption have been verified experimentally as shown on Figure 8 that plots the thrust coefficient as a function of J and RPM, and its linear regression plane corresponding to the above model.

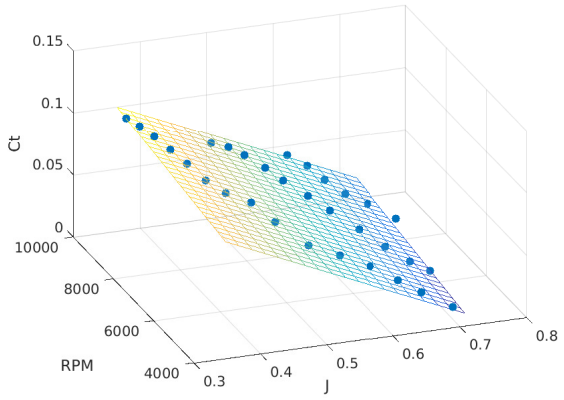

Fig. 8: Thrust coefficient (C_T) as a function of advance ratio (J) and RPM. The plane is showing a multiple linear regression of C_T over these two coefficients.

The tested configurations are all using the same motor (*AXI-2212/26*) with different propellers (glass reinforced *HQprop* propellers, see Figure 9) identified by the number of blades, the diameter (in inches) and the pitch (in inches):

- 2 blades, 8x5
- 2 blades, 6x4.5
- 2 blades, 5.5x4.5
- 3 blades, 5x4.5
- 3 blades, 4x4.5

Fig. 9: Propellers evaluated during the experiments.

prop	C_{T0}	C_{TJ}	C_{TRPM}	R^2
2_8x5	1.565e-01	-2.320e-01	3.260e-06	0.9907
2_6x4.5	1.856e-01	-2.139e-01	1.524e-06	0.9882
2_5.5x4.5	2.032e-01	-2.320e-01	-1.271e-07	0.9896
3_5x4.5	2.749e-01	-2.617e-01	-6.336e-07	0.9362
3_4x4.5	2.942e-01	-2.580e-01	1.846e-06	0.8700

Tab. 1: Results for C_T.

prop	C_{P0}	C_{PJ}	C_{PRPM}	R^2
2_8x5	9.045e-02	-1.097e-01	2.453e-06	0.9782
2_6x4.5	1.542e-01	-1.363e-01	1.497e-06	0.9760
2_5.5x4.5	1.306e-01	-1.247e-01	1.686e-06	0.9675
3_5x4.5	2.484e-01	-2.108e-01	2.381e-06	0.9864
3_4x4.5	3.358e-01	-2.559e-01	7.290e-06	0.9657

Tab. 2: Results for C_P.

prop	C_{Q_0}	C_{Q_J}	$C_{Q_{RPM}}$	R^2
2_8x5	1.440e-02	-1.746e-02	3.904e-07	0.9782
2_6x4.5	2.455e-02	-2.170e-02	2.383e-07	0.9760
2_5.5x4.5	2.078e-02	-1.985e-02	2.683e-07	0.9675
3_5x4.5	3.953e-02	-3.356e-02	3.789e-07	0.9864
3_4x4.5	5.344e-02	-4.073e-02	1.160e-06	0.9657

Tab. 3: Results for C_Q.

The results are presented in Tables 1, 2 and 3, with the coefficient of determination R^2 for each of the linear regressions. These results are matching over data found in the literature [8], validating the methodology.

It is important to note that typical values for the advance ratio J are between 0.3 and 1, while the RPM is between 3000 and 10000 rotations per seconds. So, the magnitude difference between the two is around 10^5, which is also the

magnitude difference between the $C_{\_J}$ and $C_{\_RPM}$ coefficients. The conclusion is that, in most cases, the effect of *RPM* is as great as J, while the literature usually only consider the relation with J. The main reason is probably that for larger motors, propellers and flight speeds, the effect of the Reynolds (and hence *RPM* assuming over parameters mostly constant) is less important.

Complete raw value plots of the *HQprop 8x5* propeller are presented in Appendix A.

4.2 *Relation between Aerodynamic Power and Electrical Power*

In addition to the equations presented in section 2, let's define the propulsive power as the product of the thrust and the flight speed,

$$P_{aero} = V\,T \tag{20}$$

and recall the electrical power,

$$P_{elec} = iv \tag{21}$$

The total energy of the system is then the ratio between this two values, and is mainly a function of the speed:

$$\eta_{tot}(V) = \frac{P_{aero}}{P_{elec}} \tag{22}$$

Data analysis have shown that P_{aero} and P_{elec} have a linear relation relatively independent of the speed V in the usual flight speed range of the considered UAVs. This can be seen in Figure 10.

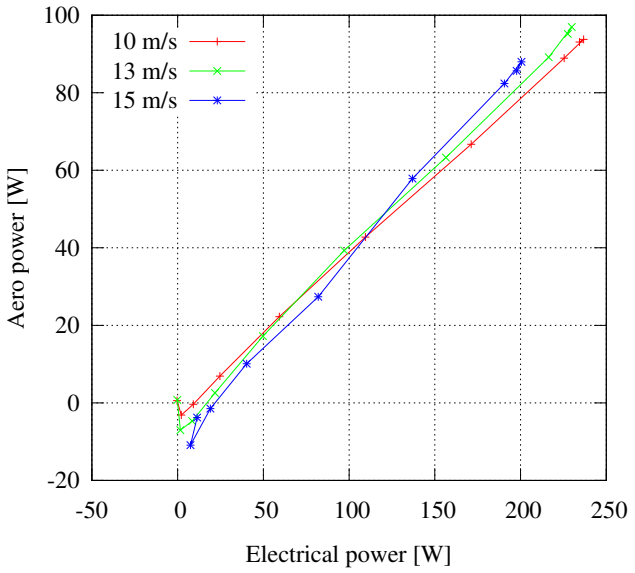

Fig. 10: Propulsive power as a function of input electrical power.

This relation is very useful since the electrical power can be easily measured by on-board voltage and current sensors. Thus, an estimation of the aerodynamic propulsive power can be used in control or other estimation algorithms involving the aircraft model. The linear model is defined as follow:

$$P_{aero} = a\,P_{elec} + b \tag{23}$$

Results are presented in table 4.

prop	a	b	R^2
2_8x5	0.4780	-9.554	0.9527
2_6x4.5	0.4287	-7.355	0.9584
2_5.5x4.5	0.4630	-7.514	0.8826
3_5x4.5	0.4303	-7.683	0.8604
3_4x4.5	0.3718	-6.876	0.7468

Tab. 4: Results for P_{aero} as a function of P_{elec}.

By looking at the data, it can be seen that the b coefficient is rather small compared to the magnitude of P_{aero} and P_{elec}. By neglecting it, the coefficient a, corresponding to the slope of the curve, is then equal to total efficiency η_{tot}. As expected, larger propellers have a better efficiency. In the case of smaller ones, the correlation factor is decreasing, which means that the assumption of linear relation being independent of the speed may not be valid anymore, or only valid for a smaller speed range.

5 Conclusion

This article have presented a test bench that is build in order to characterize the propulsion sets of small UAVs. The design is an improvement of an earlier version in order to get better and more stable results.

The presented results are covering thrust, power and torque coefficients, as well as propulsion sets efficiency and some useful relations. They can be used by researchers and engineers both during the aircraft design phase and for UAV control.

Only five propellers with the same motor have been studied so far, but the calibration and measurement procedure have been validated, and further experiments will be done.

Acknowledgments

The *SkyScanner* project is founded by the RTRA-STAE foundation.

References

[1] Mark Drela. First-order dc electric motor model. Technical report, MIT, Aero and Astro, February 2007.

[2] S. Lacroix, G. Roberts, E. Benard, M. Bronz, F. Burnet, E. Bouhoubeiny, J.-P. Condomines, C. Doll, G. Hattenberger, F. Lamraoui, A. Renzaglia, and C. Reymann. Fleets of enduring drones to probe atmospheric phenomena with clouds. In *European Geosciences Union General Assembly 2016*, 2016.

[3] Murat Bronz, Gautier Hattenberger, and Jean-Marc Moschetta. Development of a long endurance mini-uav: Eternity. *International Journal of Micro Air Vehicles*, 5(4):261–272, 2013.

[4] Murat Bronz, Jean-Marc Moschetta, and Gautier Hattenberger. Multi-Point Optimisation of a Propulsion Set as Applied to a Multi-Tasking MAV. In *IMAV 2012, International Micro Aerial Vehicle Conference and Competition*, Braunschweig, Germany, July 2012.

[5] Jean-Philippe Condomines, Murat Bronz, Gautier Hattenberger, and Jean-François Erdelyi. Experimental wind field estimation and aircraft identification. In *IMAV 2015: International Micro Air Vehicles Conference and Flight Competition*, Aachen, September 2015.

[6] Mark Drela. Dc motor and propeller matching , lab 5 lecture notes. Technical report, MIT, March 2005.

[7] McCormick B.W. *Aerodynamics, Aeronautics & Flight Mechanics*. John Wiley & Sons, Inc., 1979.

[8] Robert W Deters, Gavin K Ananda, and Michael S Selig. Reynolds number effects on the performance of small-scale propellers. In *Procedings of 32nd AIAA Applied Aerodynamics Conference, American*, 2014.

APPENDIX A HQPROP 8X5 MEASUREMENTS

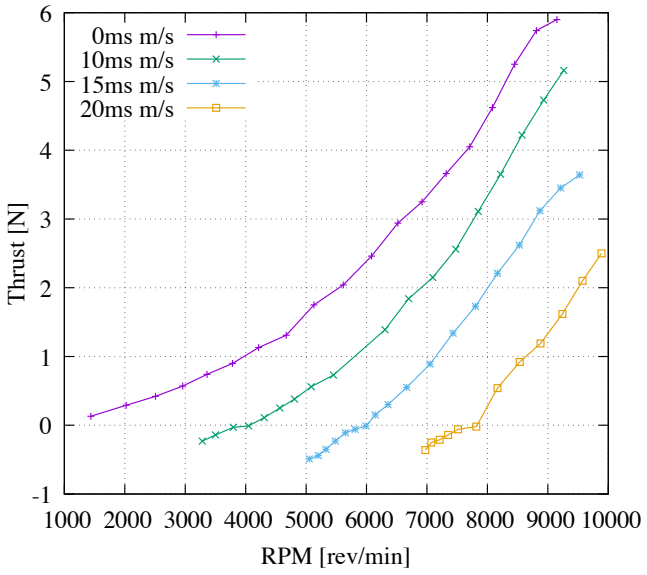

Fig. 11: Thrust vs RPM

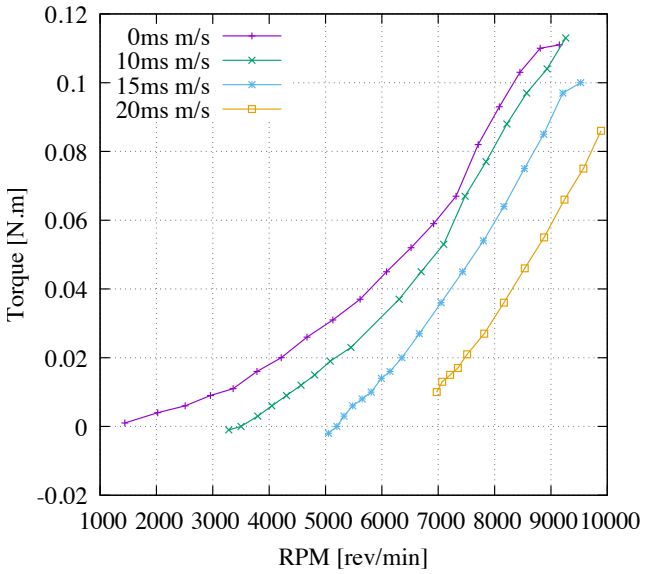

Fig. 12: Torque versus RPM

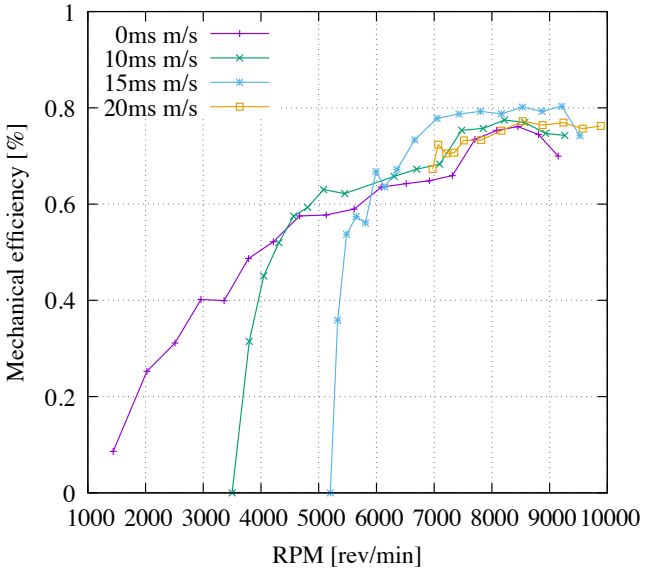

Fig. 13: Mechanical efficiency versus RPM

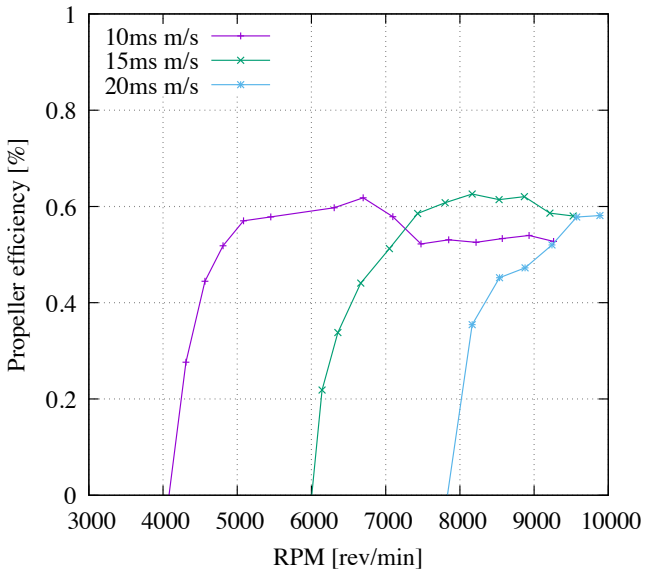

Fig. 14: Propeller efficiency versus RPM

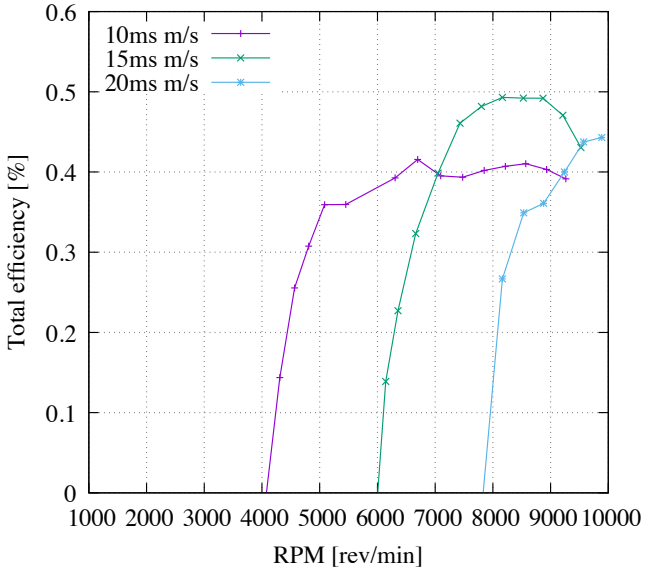

Fig. 15: Total system efficiency versus RPM

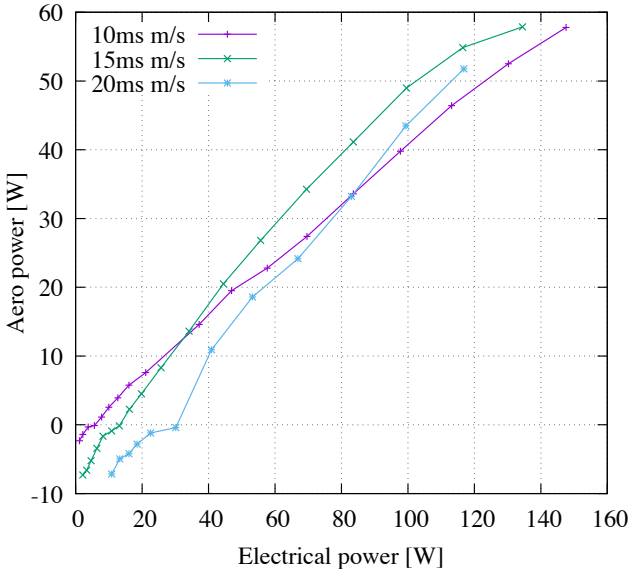

Fig. 16: Propulsive power versus electrical input power